Volume 28
Number 2
12 January 2026
Pages 293–596

CrystEngComm

rsc.li/crystengcomm

ISSN 1466-8033

ROYAL SOCIETY OF CHEMISTRY

PAPER
Jerry Y. Y. Heng *et al.*
The effect of solvents on crystal regeneration

CrystEngComm

PAPER

View Article Online
View Journal | View Issue

Cite this: *CrystEngComm*, 2026, **28**, 357

The effect of solvents on crystal regeneration

Isha Bade, Deniz Etit and Jerry Y. Y. Heng *

Received 31st March 2025,
Accepted 20th September 2025

DOI: 10.1039/d5ce00353a

rsc.li/crystengcomm

Solvents play a pivotal role in crystallisation, affecting crystal growth and properties. This study investigates the regeneration behaviour of paracetamol crystals in ethanol, tetrahydrofuran, and acetone using both evaporative and isothermal crystallisation setups, coupled with a custom MATLAB-based edge detection algorithm for facet-specific growth rate measurements. Regeneration was observed in all solvents, with the fastest rate observed in ethanol (0.07 mm h^{-1}), followed by THF (0.03 mm h^{-1}), and acetone (0.02 mm h^{-1}) at a supersaturation ratio of 1.10. In all cases, regeneration was driven by rapid growth of the (0 1 0) facet, restoring crystals to their original shapes. Crystal shape influenced the regeneration time, with a rapid initial phase comprising 8–15% of total regeneration time. Molecular dynamics simulations were utilised to quantify solvent–crystal interactions, showing that not only do the inherent solvent properties play a role but also the solubility of paracetamol significantly affects crystal regeneration.

Introduction

Morphology defines the inherent and unique set of crystal faces, resulting from the crystals' internal structure. While the equilibrium morphology, based on the Gibbs–Wulff theorem,[1–3] is governed by thermodynamics, solution-grown crystals rarely achieve such ideal conditions due to the complex interactions in the liquid phase. The morphology of solution-grown crystals is determined by kinetics, such that the steady-state morphology will be dominated by the slow growing facets, as established by Frank and Chernov.[4–6] This is because in a solution environment, the attachment of growth units onto the crystal surface defines the particle shape rather than the surface tension. Traditional models like the Bravais–Friedel–Donnay–Harker (BFDH)[7–10] and attachment energy (AE)[11,12] theories provide insight into kinetic morphology based on the interplanar spacing and periodic bond chains respectively, however, are calculated in a vacuum environment and overlook solvent effects. To address this limitation, modified attachment energy (MAE)[13,14] models and molecular dynamics (MD)[15,16] simulations have been developed, incorporating solvent–crystal interactions to better predict real-world crystal growth.

The use of different solvents has been shown to alter crystal habit whilst maintaining the same polymorphic form and therefore influencing downstream processibility of crystals such as filtration, compatibility and flowability.[4,17–19] As different crystal facets have different chemical moieties,[20–22] the solute–solvent interactions for each facet vary, leading to different facet specific growth rates and eventually a solvent-specific crystal habit. For form I paracetamol specifically, various studies have reported solvent-specific habits attributing to solvent properties such as polarity, pH, solubility of the solute, and the hydrogen bonding interactions between the solute and the surface chemical groups.[23–26] For example, experimental studies with paracetamol have demonstrated a columnar habit when using polar protic water, and a prismatic habit in other selected polar protic, aprotic, and non-polar solvents.[23] Multiple studies have also validated experimental findings using molecular dynamic simulations where the solute–solvent interactions on different facets have been computed.[16,27–30] However, these investigations are limited to the most morphologically important facets – facets that occupy the highest surface area of the equilibrium crystal habit. The effect of solvents on the facets exposed after breakage is seldomly studied even though breakage can drastically affect the final crystal properties.

Mechanical breakage is commonly observed in industrial crystallisers due to crystal–crystal, crystal–impeller, and crystal–wall interactions.[31] Approaches to determine crystal morphology have evolved over the years, as seen above, but surprisingly very little is known and studied about the effect of mechanical breakage on the final crystal structure, shape and size. Population balance models (PBMs) generally do not account for breakage and growth post breakage due to the added complexity as well as the lack of experimental data on the topic.[32,33] In the last decade, models have been developed that take into account crystal fragmentation and their consequent growth,[34,35] as well as simultaneous crystal shape and size prediction.[4,32,36] However, none of these models take into consideration specific post breakage growth kinetics, and assume that growth of fragments will follow the same

Department of Chemical Engineering, Imperial College London, South Kensington Campus, SW7 2AZ, UK. E-mail: jerry.heng@imperial.ac.uk

trajectory as unbroken crystals. Very recently, steps have been taken in understanding the facet development of fractured crystals through 4D tracking in studies observing the growth of fractured aluminium potassium sulphate crystals.[37] Additionally, simulations have been employed to predict the growth rates of the facets of *para*-aminobenzoic acid crystals exposed by breakage.[38] On the process modelling side, an MSMPR model has been developed, designed to utilize broken crystals as seeds as a means of enhancing product yield due to their faster growth rates than unbroken crystals.[39] However, still, large knowledge gaps exist in the understanding of the specifics of the post-breakage crystal growth behaviour due to a lack of experimental evidence. Recently, the 'regeneration' phenomenon was reported for the first time where in a paracetamol crystal was observed to grow back to its original shape after breakage along its cleavage plane (0 1 0), before demonstrating overall growth.[40] Consequently, instances of regeneration were reported by other research groups in the past year, both in paracetamol crystals[41] and other systems, such as aceclofenac.[42]

Single crystal growth rate measurements have been of interest for many years. By growing high-quality single crystals and precisely measuring their dimensions, researchers can elucidate crystal growth behaviour in extreme detail, which can then be applied to multi-crystal and bulk systems. Traditionally, single crystal growth cells equipped with real-time microscopy have been widely used to capture crystal growth.[43–45] While early analyses relied on manual measurements, recent advancements have introduced edge detection algorithms for more automated assessments.[45,46] However, these growth cells are limited to stagnant systems without stirring. To overcome this limitation and collect growth data from multiple crystals, a rotating disk method was developed, where crystals are immobilised on an impeller rotating at a controlled speed.[47,48] However, this approach does not allow real-time imaging—crystal dimensions can only be measured before and after the experiment. Despite these advancements, real-time single crystal imaging remains highly desirable yet challenging and labour-intensive. Moreover, all these methods typically use extremely small crystals, where growth occurs within minutes to hours, making it difficult to capture subtle or uncommon phenomena. To address this, the authors introduced a new methodology,[40] employing macrophotography to study the growth of larger, high-quality crystals. This approach enables slow and precise real-time tracking of crystal growth.

The work investigates the effect of three different solvents; ethanol, tetrahydrofuran (THF) and acetone, on the regeneration behaviour of paracetamol crystals, providing mechanistic insights into the post breakage growth phenomenon. The rate of regeneration in each system was measured using automated real-time imaging and image analysis techniques developed in-house. Interaction energy calculations between the (0 1 0) surface and the solvent molecules were also performed computationally, elucidating the trends in solvent-specific regeneration rates.

Experimental section

Materials

Paracetamol (CAS: 103-90-2) with >98.0% purity was purchased from Sigma Aldrich. Ethanol (CAS: 64-17-5) with 99.8% purity and acetone (CAS: 67-64-1) with 99.8% purity were purchased from VWR Chemicals. THF (CAS: 109-99-9) with 99.8% purity was purchased from Thermo Scientific.

Obtaining and cutting crystals

Single crystals in ethanol, acetone, and THF were obtained *via* slow solvent evaporation at room temperature. A saturated solution of paracetamol and the desired solvent at room temperature was prepared and filtered through a 0.45 μm PTFE filter into a 50 ml borosilicate glass crystallisation dish. Once the dish was three quarters of the way full, it was covered using parafilm which was pierced using tweezers to make approximately 1 mm diameter perforations. It was then placed in the fume hood to allow for slow evaporation of the solvent. After having left the crystallisation dish in the fume hood for a few days, depending on the rate of evaporation of the solvent, approximately 1–2 mm diameter seeds of paracetamol could be seen at the base of the dish. These seeds were carefully collected using blunt tweezers, immediately placed on a soft tissue and pat dried to avoid encrustation on the crystal surface. The seed crystals were placed individually in small vials, filled with ~10 ml of saturated solution of the corresponding solvent. The vials were covered with parafilm, perforated as mentioned above and placed in the fume hood for 1 week to enable evaporative crystallisation. The solution was continually refilled so that the vials do not dry out during the experiment. Once the crystals reached an approximate size of 4–5 mm, they were collected and dried using the same procedure mentioned above. To conduct the regeneration experiments, prepared paracetamol crystals were cleaved along their (001) facets, exposing their internal cleavage plane (0 1 0), using the same methodology as detailed in the previous publication[40] and as seen in Fig. 1(a).

Powder XRD

Powder X-Ray Diffraction (PXRD) investigation for the crystals obtained from the three solvents was carried out using PANalytical X'Pert PRO X-ray diffractometer. As standard PXRD protocol, the crystals were ground to fine powder in a pestle and mortar to minimise any preferred orientation. The powder was then pressed flush against the sample holder using a glass slide to flatten it and excess powder on the edges of the holder was brushed off using soft tissue prior to being placed inside the machine. The X-ray diffraction measurement was performed using Cu Kα radiation (1.5405 Å) at 40 kV and 20 mA. All samples were conducted at a scanning rate of 50 seconds per step, with a step size of 0.013°, over a diffraction angle range from 5° to 35°.

The PXRD pattern for form I paracetamol was calculated in Mercury (version 2024.1.0, CCDC, Cambridge, U.K.) using

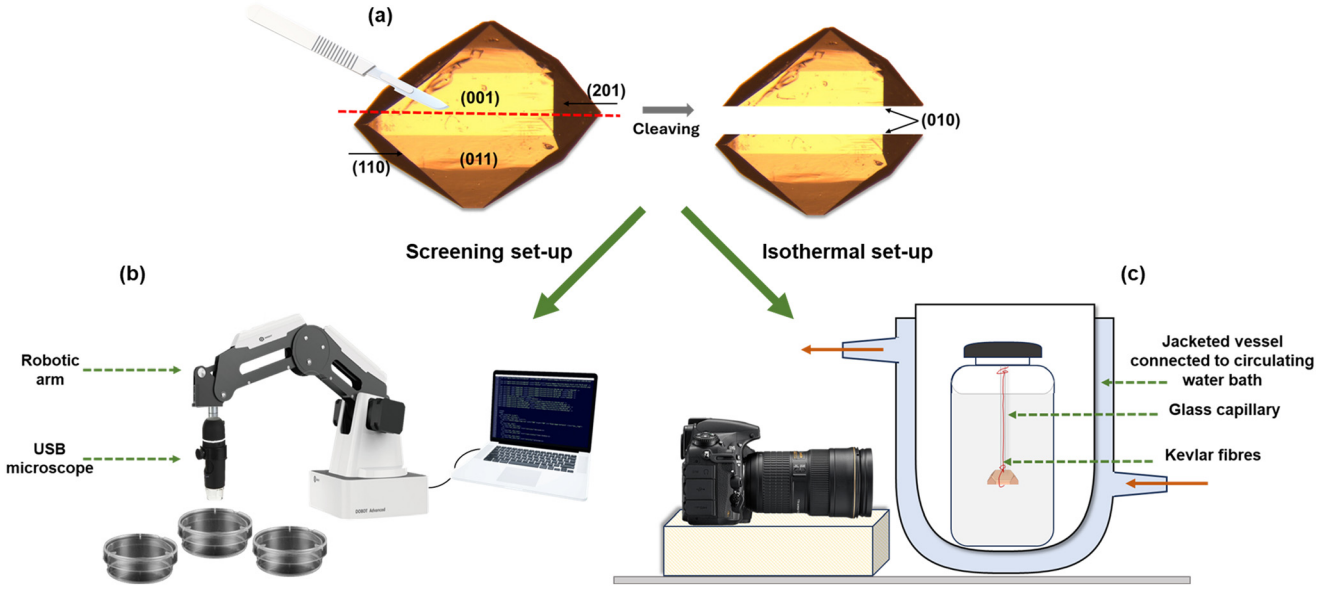

Fig. 1 Experimental setup depicting the (a) cleaving process of a paracetamol crystal, and the 2 imaging setups; (b) automated screening using robotic arm for evaporative crystallisation, (c) isothermal crystallisation with DSLR camera.

the crystal structure data deposited in the Cambridge Structural Database (CSD), reference: HXACAN01.[49]

Automated setup for regeneration screening

An automated imaging setup was built using an RS90 USB microscope attached to a DoBot® magician robotic arm that was programmed using a Python script, to screen multiple crystallisation dishes over a certain period (Fig. 1(b)). 50 ml crystallisation dishes were filled with a saturated solution of paracetamol–solvent (acetone, ethanol, or THF) at room temperature and paracetamol crystals grown from the respective solvent were cleaved and placed in the dish. The dishes were covered using a glass lid with an overhang of 5 mm, allowing very slow solvent evaporation and hence crystal growth. With the aid of the robotic arm, the microscope was able to move over the dishes at regular time intervals and capture images. These images were then analysed using an edge detection script developed in-house using MATLAB, detailed below, to obtain growth rate data.

Regeneration at constant supersaturation

Solubility curve for paracetamol in different solvents. The solubility of paracetamol in ethanol, acetone and THF at six different temperatures; 10 °C, 20 °C, 25 °C, 30 °C, 40 °C and 50 °C were measured *via* gravimetric analysis. 100 ml of solvent was mixed with an excess of paracetamol and stirred using a magnetic stirrer at the desired temperature at 200 rpm for 24 hours. The solution was then allowed to settle for two hours, following which two 5 ml samples were taken and filtered through 0.2 μm cellulose acetate membrane into Eppendorf vials. The solution from the vials was then allowed to evaporate at room temperature until no traces of liquid were left. The mass of the solution before and after evaporation was measured and the concentration of the solution was calculated using eqn (1).[50]

$$c = \frac{(m_{vdr} - m_v)}{(m_{vs} - m_{vdr})} \quad (1)$$

where m_{vdr} is the combined mass of the dried solute and the vial, m_{vs} is the combined mass of the solution and the vial, and m_v is the mass of the empty vial. This was repeated thrice for each temperature and hence an average concentration over six samples was calculated to determine the solubility curve. The final solubility curve; concentration against temperature, was found by fitting the data points as an exponential function of temperature with an R^2 value closest to 1.

Isothermal crystallisation. To investigate the effect of solvents at a constant supersaturation an isothermal crystallisation setup was developed (Fig. 1(c)). A 100 ml jacketed vessel was connected to a circulating water bath. Paracetamol crystals of size of 4–5 mm were cleaved and suspended in a 60 ml glass bottle, ensuring the freshly cleaved facet faced the bottle's base. It is important to note that just after cleaving the crystal, it is washed with ice cold water (4 °C) and gently pat-dried with tissue. Given the very low solubility of paracetamol in water at 4 °C (~0.01 g g^{-1}), this step was considered effective for removing any debris and minimising secondary nucleation. The crystal was immobilised by tying it to a few strands of Kevlar fibre, threading these fibres through a glass capillary, and securing the fibres to the capillary using Blu Tack®. The capillary was passed through a hole in the bottle lid and secured in place, again using Blu Tack®. This immobilised the crystal in the solution for better imaging, as seen in Fig. 1(c). Initially, a solution saturated at 30 °C (T_0) was added to a glass jar,

which was then placed in the jacketed vessel set at 30 °C for 2 hours.

The solution was subsequently cooled to a temperature resulting in a supersaturation ratio of 1.10 (T_c) and maintained for another hour, after which the crystal was inserted into the solution. The insertion of crystal was done with great care to prevent any sudden disturbance to the crystal which could potentially serve as a reason for nucleation. The supersaturation ratio, S, was calculated using the solubility data using eqn (2):

$$S = \frac{c}{c^*} \quad (2)$$

where c is the concentration of the solution, and c^* is the equilibrium concentration (solubility) at a given temperature.

The jacketed vessel was placed inside a photography light box and using the same Nikon D90 DSLR camera rig detailed in the previous study,[40] the regeneration of the crystals was monitored. Images were captured every 15 min for a duration of 55 hours following which they were analysed using an in-house MATLAB script, detailed in the results below, to obtain growth data. It is important to note that concentration of the solution was measured before the crystal was inserted as well as at the end of the 55 hours. In each case the change is concentration was ≤5% and therefore considered constant throughout the experiment.

Measuring crystal growth rate

A MATLAB script was developed to process and analyse the images from both set of experiments; screening with robotic arm, and isothermal crystallisation. The script is essentially an edge detection algorithm that traces the crystal boundary and can be used to obtain desired dimensions of the crystal. Two types of measurements were obtained:

1. Characteristic lengths: for the screening studies, two characteristic dimensions of the crystal were measured; length a, normal to the cleavage plane, and length b, parallel to the cleavage plane (Fig. 2(a)). This approach has been described in detail in the previous publication.[40]

2. Facet propagation of (0 1 0): for the isothermal crystallisation studies, to get a more accurate representation of the rate of regeneration, the advancement of the (0 1 0) was measured (Fig. 2(b)).

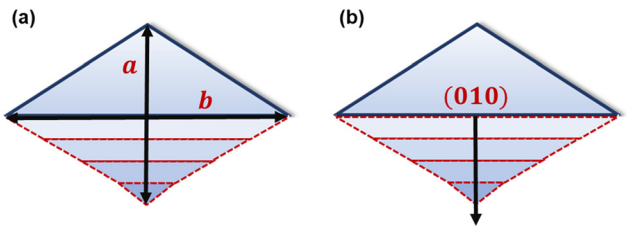

Fig. 2 Diagram depicting the measurement of (a) characteristic dimensions: length a and b (b) facet propagation of (010) on a simplified drawing of a paracetamol crystal as viewed through the microscope and camera.

The crystal growth rate was then calculated using the following equation (eqn (3)):

$$G = \frac{\Delta L}{\Delta t} \quad (3)$$

where L is the length of the characteristic dimension or the distance between the crystal centre and the facet (hkl), and t is the time.

Fig. S1 depicts a summary of the image analysis script for a representative crystal image. A summary of the key steps of the algorithm can be found in the SI whilst the full script is available to readers upon request.

Computational section

For all computational studies, crystal structure of monoclinic form I paracetamol was obtained from the Cambridge Structural Database (CSD) (refcode: HXACAN01 (ref. 49)), of space group $P2_1/a$ with lattice parameters: a = 12.93 Å, b = 9.40 Å, c = 7.10 Å and α = 90°, β = 115.9°, γ = 90°, with four paracetamol molecules in the unit cell. All simulations were performed in Accelrys Materials Studio 7.0 software.

Forcefield selection

Prior to any simulations, the crystal structure was geometry optimised using the 'Forcite' module using 3 forcefields: COMPASS II,[51] Drieding,[52] and Universal,[53] that are commonly used for organic molecules. COMPASS II was chosen as the forcefield going forwards as the relative error associated with the optimised cell parameters was the least (Table S2).

Vacuum morphology

Following geometry optimisation, the crystal habit in vacuum was predicted using the 'Morphology' tool in Materials Studio. The 'Growth Morphology', which is based on the attachment energy (AE) model, was executed using the COMPASS II forcefield and a list of important facets that determine the morphology was obtained.

Interaction energy calculation

Based on the vacuum morphology, the crystal was cleaved parallel to the (0 1 0) surface and a periodic supercell of 3 × 3 unit cells and 4 × d_{hkl} depth was created. The solvent layer was then constructed using the 'Amorphous cell' tool by creating a cell of 400 randomly distributed solvent molecules of the desired solvent; ethanol, acetone, and THF. The dimensions of the solvent layer were chosen to match that of the superstructure of the crystal surface and the target density was set to the solvent density at room temperature (298 K): ethanol – 0.789 g cm^{-3}, acetone – 0.784 g cm^{-3}, and THF – 0.888 g cm^{-3}. The amorphous layer was then subject to geometry optimisation and cell relaxation by molecular dynamics using the NVT ensemble at 298 K for 300 ps controlled

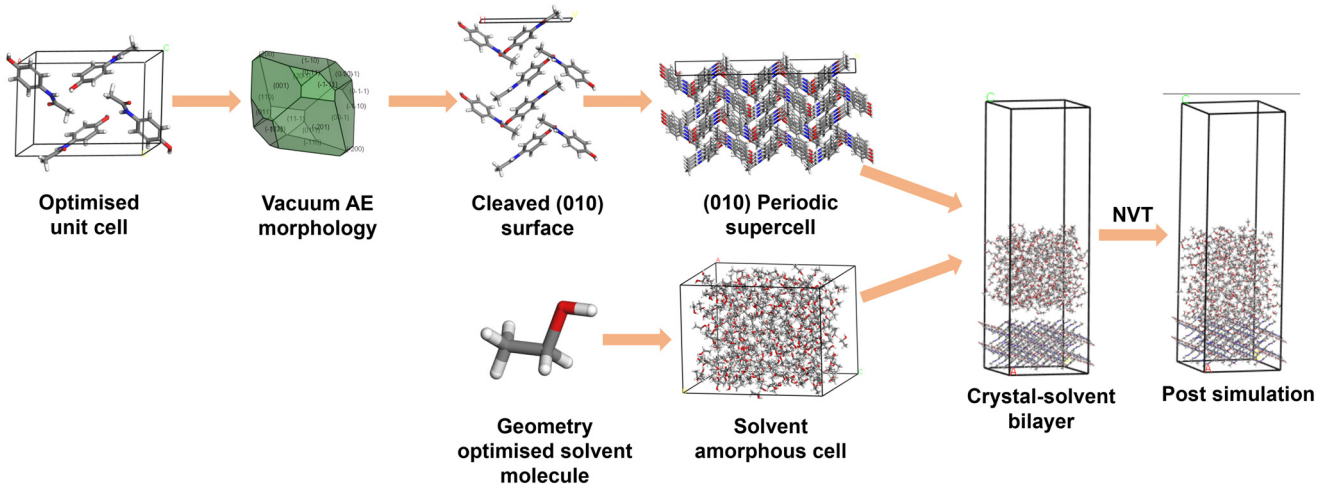

Fig. 3 Flowchart illustrating the workflow utilised in Materials Studios for evaluating surface-solvent interaction energy.

by the Anderson thermostat.[54] The NVT ensemble ensures that a constant number of moles, volume, and temperature of the system is maintained. Subsequently, a bilayer was built with the solvent layer placed above the crystal surface along the *c* axis. A 50 Å vacuum slab was placed above the solvent layer to avoid the effect of additional free boundaries. All except the topmost layer of the crystal were fixed along the *a*, *b*, and *c* directions. The entire system was then geometrically optimised, and the MD was assessed by the Anderson thermostat using the NVT ensemble at 298 K with a step time of 1 fs. The electrostatic interactions were calculated using the Ewald method with an accuracy of 0.0001 kcal mol^{-1}, whilst the atom-based summation method with a cut-off distance of 15.5 Å was used for van der Waals forces. Two sets of MD simulations were run, first to equilibrate the whole system for 100 ps (Fig. S2) followed by another MD simulation for 50 ps to obtain the energy values. Fig. 3 shows a schematic representation of the simulation approach for this study, whilst dimensions of the unit cell of the (0 1 0) surface as well as the simulation box can be found in Table S3.

The total potential energy, E_{tot}, of the simulated crystal–solvent layer was used to the calculate the interaction energy, E_{int}, using eqn (4):

$$E_{int} = E_{tot} - (E_{cry} + E_{sol}) \quad (4)$$

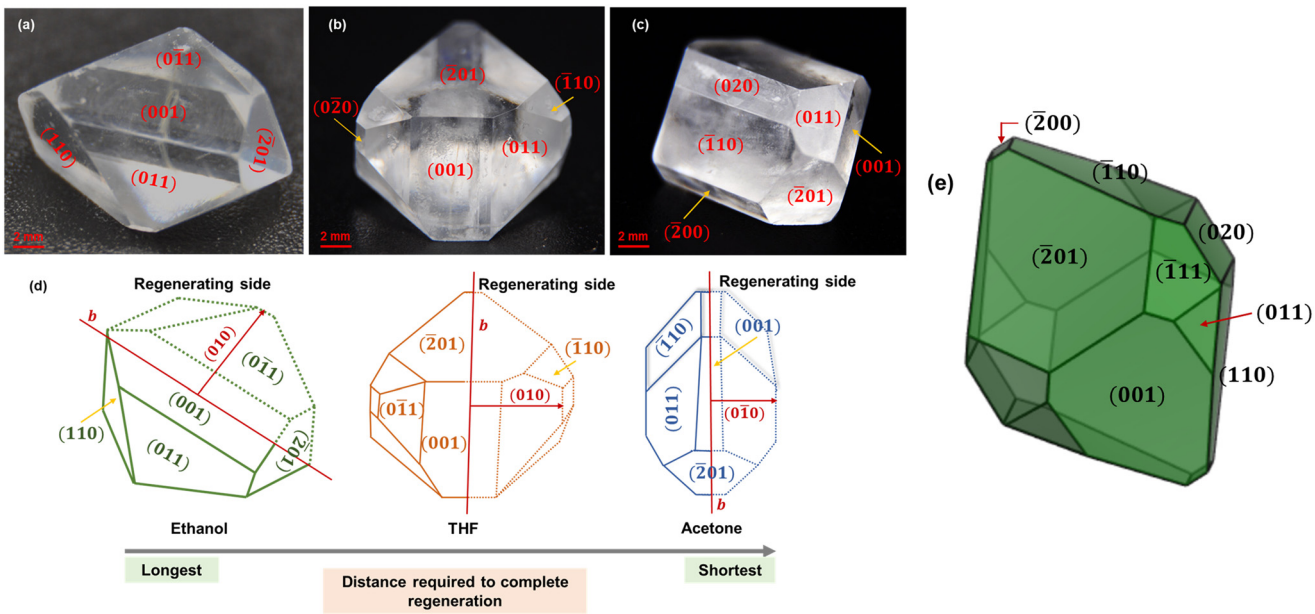

Fig. 4 Experimental habits of paracetamol obtained *via* slow evaporation in (a) ethanol, (b) THF, and (c) acetone. The crystals in the image are approximately 1 cm large along their longest dimension (d) diagrams highlighting the characteristic dimension b and (010) facet propagation on the observed experimental habits in the different solvents (e) vacuum habit of form I paracetamol (HXACAN01) predicted by the attachment energy theory using Materials Studio.

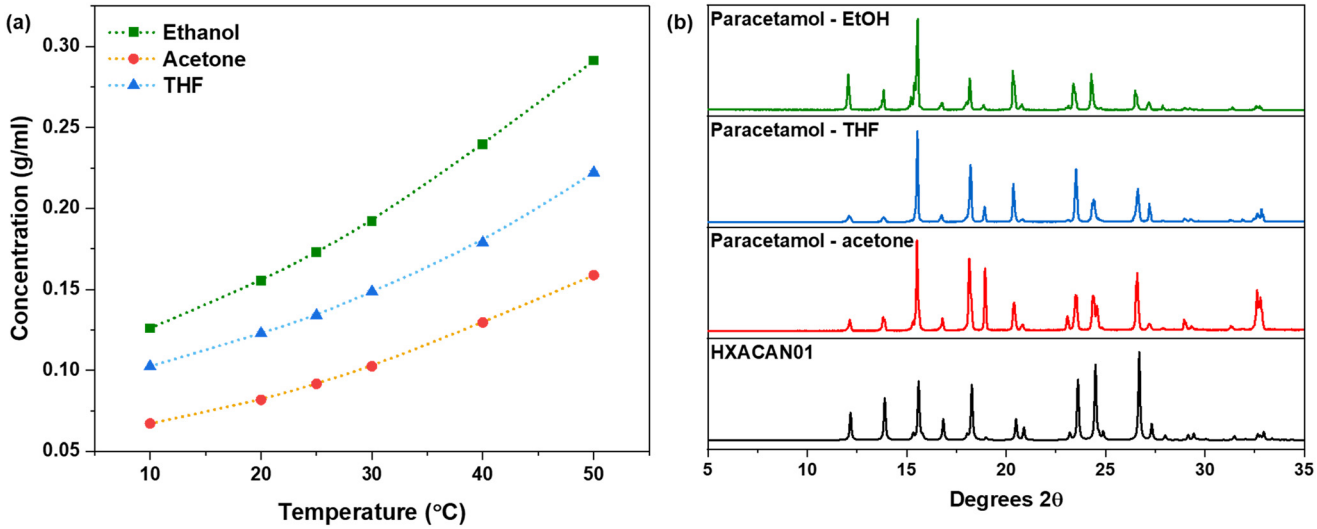

Fig. 5 (a) Solubility curves of paracetamol in the three solvents and (b) diffraction patterns of crystals obtained from top to bottom: ethanol, THF, and acetone, compared to the diffraction pattern of form I paracetamol (HXACAN01) obtained using Mercury.

where E_{cry} and E_{sol} are the energy of the crystal and solvent layer respectively.

Results

Experimental habits and PXRD patterns of paracetamol from different solvents

Experimental habits of paracetamol crystals obtained from ethanol, acetone and THF solutions can be seen in Fig. 4(a–c). PXRD confirmed the crystals to be of the monoclinic form I paracetamol (Fig. 5(b)). However, the habits are seen to be relatively different. Although they are of the same polymorphic form and have the same major facets, in agreement with the attachment energy habit shown in Fig. 4(e), the proportion of facets occupied on the equilibrium habit varies, highlighting the significance of solvent effects on the crystal growth. For instance, even though facets (1 1 1) and (2 0 0) appear on the attachment energy habit, due to the fast-growing nature of the facets, (1 1 1) does not appear on any experimental habits whilst (2 0 0) only appears on crystals grown in acetone. Overall, the experimental habits are in line with the 'prismatic' morphology reported in literature.[23,43]

Solubility curve of paracetamol in ethanol, acetone, THF

The solubility curves of paracetamol in ethanol, acetone and THF can be found in Fig. 5(a) and show good agreement with literature.[50] Paracetamol shows highest solubility in ethanol, followed by THF, and the lowest in acetone. As the standard deviation (SD) of the solubility data is less than 2% and cannot be seen clearly on the plot, the corresponding SD values can be found in the supplementary information (Table S1), along with the equations of the respective solubility curves. Using the measured solubility at 30 °C, the concentration resulting in a supersaturation of 1.10 was calculated *via* eqn (2), for each solvent system. Consequently the temperatures corresponding to a supersaturation of 1.10 for ethanol, acetone, and THF were found and can be seen in Table 1 below.

Regeneration screening results from 3 solvents

Regeneration was previously observed and reported in ethanol.[40] Here, cleaved paracetamol crystals were also screened for regeneration in acetone and THF, and growth developments from all three solvents were compared. The results, including the visual developments and the quantified growth trends, are respectively provided in Fig. 6 and 7. Fig. 7(a(ii))–(c(ii)) show the change in lengths a and b over time in ethanol, THF and acetone respectively, averaged over 3 runs, as obtained using the script. The growth rates were also analysed by categorising the growth processes into 3 stages: early-stage regeneration covering the initial half of the

Table 1 Crystallisation conditions at S = 1.10 for the regeneration of paracetamol in ethanol, acetone, and THF. Note: SD reported is $\times 10^{-4}$

Solvent	Crystallisation temperature T_c / °C	Concentration c / g ml^{-1}	Equilibrium concentration c^* / g ml^{-1}	Δc / g ml^{-1}
Ethanol	25.6 ± 0.1	0.190 ± 3.4	0.173 ± 3.1	0.017 ± 4.6
Acetone	25.9 ± 0.1	0.103 ± 1.5	0.093 ± 1.4	0.011 ± 2.1
THF	25.8 ± 0.2	0.149 ± 5.3	0.135 ± 4.8	0.014 ± 7.2

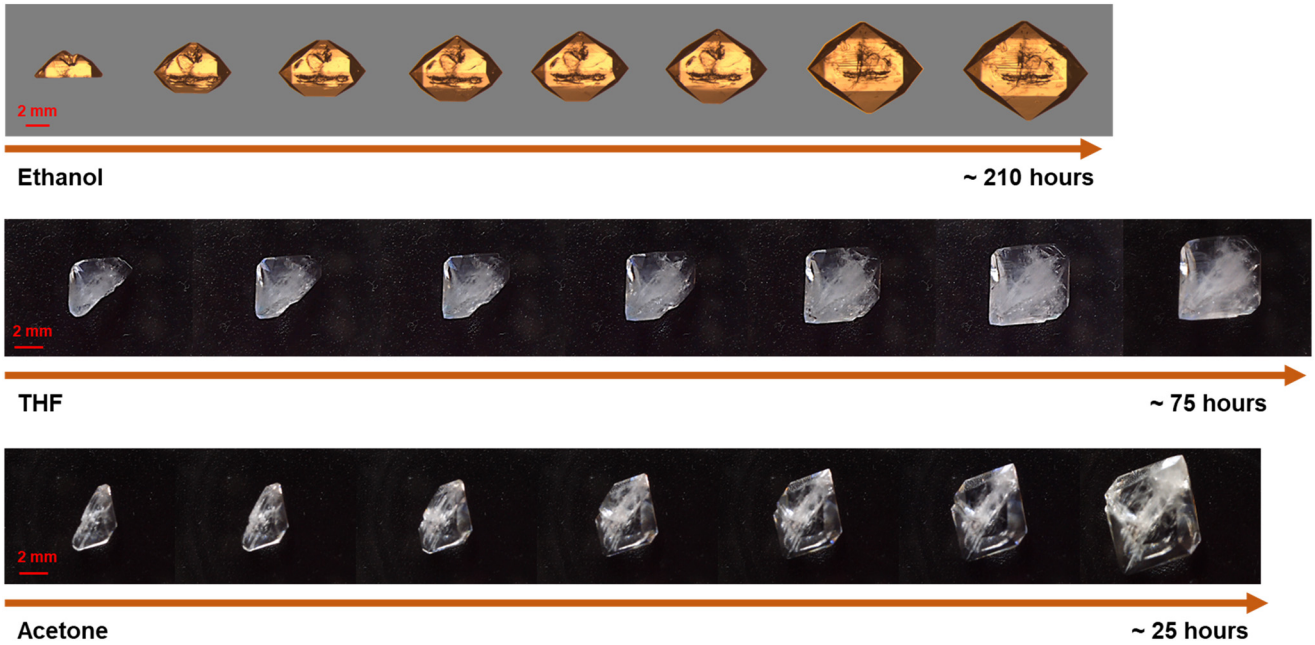

Fig. 6 Micrographs depicting the regeneration phenomenon in each solvent; top to bottom; ethanol (image adapted with permission from ref. 40), THF, acetone.

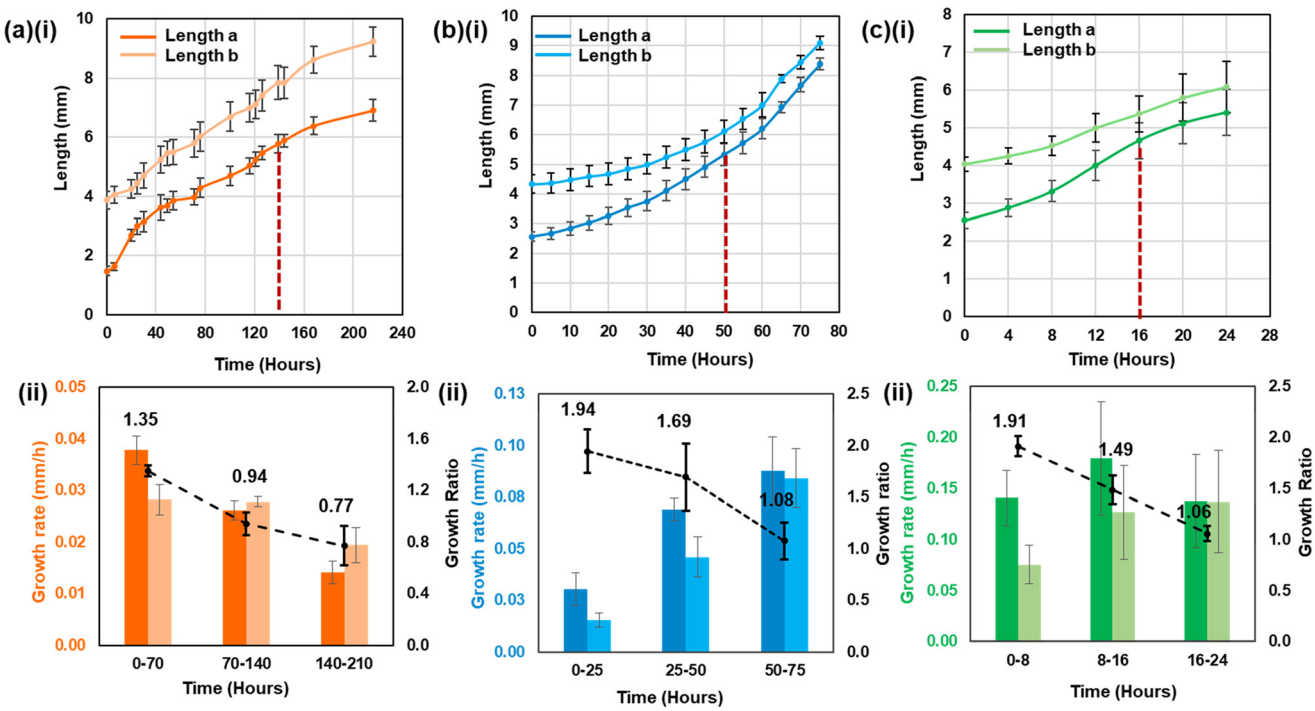

Fig. 7 Plots for (a) ethanol, (b) THF, and (c) acetone depicting the (i) change in characteristic lengths, *a* and *b*, of crystals over time, and (ii) crystal growth rate and growth ratio, for the 3 stages of growth post cleavage: rapid regeneration, sluggish regeneration and overall growth.

regeneration period, late-stage regeneration encompassing the latter half of the regeneration, and post-regeneration where an equal time is allowed to monitor the development of an unbroken crystal.

Firstly, the outcomes demonstrate that paracetamol's regeneration capability is not limited to ethanol, but it also occurs in different solvents. Therefore, the results indicate that materials that demonstrate crystal regeneration can do it in different solutions and, accordingly, from different shapes. Paracetamol regeneration took around 140 h in ethanol, 50 h in THF, and 16 h in acetone for crystals of same size.

Fig. 8 Regeneration snapshots of paracetamol in top to bottom: ethanol, THF, and acetone.

According to the 3 process stages, though the absolute rates differed, the growth rate ratio, that is the ratio of growth rates of the regenerating direction over the normal direction, was around twice in the early-stage regeneration compared to the post-regeneration period. Thus, the regenerating dimension grows rapidly during regeneration, whereas the ratio of the growth rates approach to their post-regeneration levels during the process (1.35 to 0.77 for ethanol, 1.94 to 1.08 for THF, 1.91 to 1.06 for acetone). The post-regeneration period illustrates the case of an unbroken crystal, which is related with the equilibrium shape of the crystal in the corresponding solvent.

Briefly, the evaporative crystallisation experiments provided visual evidence for a crystal's regeneration capability across different solvents, and yielded similar growth trends across the solutions. The results also indicated slightly different supersaturation levels in the current evaporative crystallisation setup. Whilst the starting supersaturation was 1 for all systems, supersaturation at the end of the experiment was measured to be 1.08 ± 0.02 for ethanol, 1.24 ± 0.19 for THF, and 1.19 ± 0.11 for acetone. Hence, it was decided to compare different solvents also in an isothermal crystallisation setup, benefiting from the temperature control the latter allows to decouple the effects of solvent–solute interactions and the level of supersaturation on regeneration.

Isothermal non-agitated crystallisation

Firstly, as seen from the snapshots in Fig. 8, paracetamol crystals were observed to regenerate in all three solvents, confirming the outcomes of the evaporative crystallisation tests. The time taken for regeneration varied across the systems with the fastest regeneration taking place in acetone, followed by ethanol, and lastly THF. To further quantify the

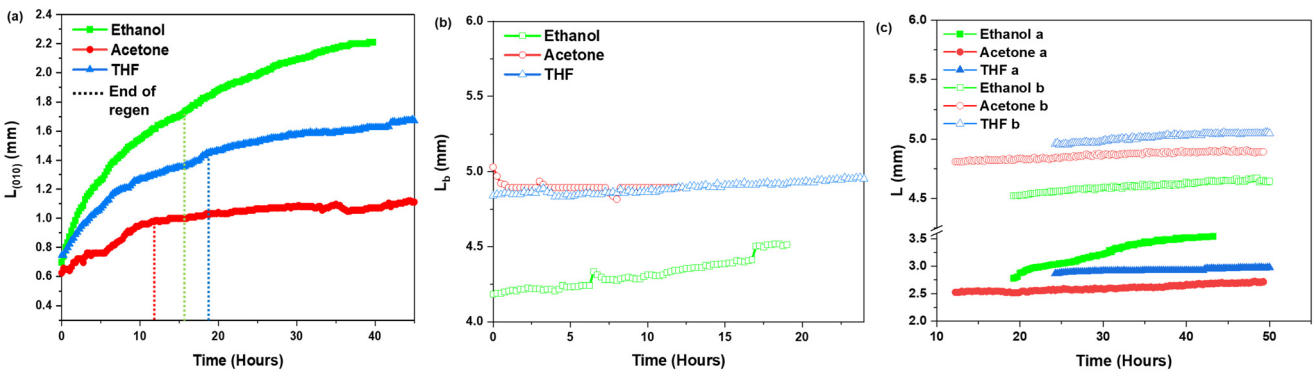

Fig. 9 Example plots of crystal growth in each solvent obtained *via* MATLAB. Each line represents 1 individual crystal: (a) facet propagation of (010) for the entire duration of the experiment. Using this plot, the duration of the fast regeneration and the total regeneration period was deduced. Change in characteristic dimensions (b) b during regeneration and (c) a and b after regeneration. The gradients of these plots were used to estimate the growth rates.

growth behaviour in the different crystallisation environments, the facet propagation of (0 1 0) was measured alongside the characteristic length *b*. Even though the dihedral angle between the (0 1 0) and (1 1 0) plane stays constant regardless of the crystal habit, the varying morphological significance of facets in different solvents leads to inconsistencies in which facets are imaged. Therefore, keeping the focus on (0 1 0), (1 1 0) is only visible in ethanol but not in acetone and THF. To keep the comparison uniform, growth rate of (0 1 0) and length *b*, *i.e.*, non-regenerating crystal dimension, for the different habits were calculated.

Fig. 9(a) show a representative plot of the data obtained using the script for the propagation of facet (0 1 0) for the entire duration of an isothermal crystallisation experiment. Using these plots and more importantly with visual verification from images, the end point of regeneration for every crystal was deduced. The point where the line shows a change in gradient as well as the images indicate full shape restoration was designated as the end point of regeneration (as seen from the long-dashed lines). Once the end point of regeneration is determined, the growth rate in mm h^{-1}, before and after regeneration, for the dimension of interest was calculated by fitting a linear trendline to the growth data. It is important to note that after regeneration is completed, (0 1 0) is no longer present on the crystal, deeming facet propagation of (0 1 0) unreliable. Therefore, post regeneration in isothermal crystallisation, length *a* and *b* are measured to demonstrate the change in characteristic dimensions of the crystal post regeneration.

The estimated regeneration rates varied between the solvents in the following order: ethanol > THF > acetone. Fig. 10(a) highlights that regeneration in ethanol was almost 3 times and 4 times faster than in THF and acetone, respectively. Moreover, just as observed in the case of evaporative crystallisation above, the facets on the unbroken side of the crystals, regardless of the habit, were relatively dormant during regeneration, and maintained a trivial growth rate in the range of 0.006–0.017 mm h^{-1}. Post regeneration, once the pre-breakage shape is restored, length *a* and length *b* grow at relatively equivalent growth rates as shown in Fig. 10(b). Interestingly, after regeneration, the trend between acetone and THF reverses, with crystal growth in acetone becoming nearly three times faster than in THF, although ethanol still leads with the fastest growth rate. It is important to note that the elongated appearance of the error bars in Fig. 10(b) is primarily due to the narrow range on the *y*-axis. Despite the standard deviation, there remains a relative difference in growth rates among the three solvents. Notably, in the case of THF, the slight negative value of the error bar of length *b* is an artifact resulting from the very slow growth rate, which overlaps with the uncertainty introduced by the edge detection algorithm.

Even though the rate of regeneration in acetone was the lowest in comparison to the other solvents, it resulted in the shortest regeneration period. This was due to the distance required for the (0 1 0) facet to grow to complete the regeneration (Fig. 4(d)). For instance, crystals grown in acetone have a very small (011) facet and a large (1 1 0) facet, opposite to that of ethanol-grown crystals. Hence, in acetone, (0 1 0) had to grow over a shorter length before the growth habit was achieved as opposed to in ethanol, where (0 1 0) had to keep growing until the large (0 1 1) facets were formed. Therefore, the time taken for regeneration was normalised over the distance of facet propagation required for regeneration to be completed. These normalised regeneration times can be seen as the blue dotted line in Fig. 10(a) and as expected depict the opposite trend to that of the regeneration rates.

It was reported previously that regeneration occurs in two steps; rapid regeneration followed by sluggish regeneration.[40] At the start of regeneration, the (0 1 0) facet grows extremely

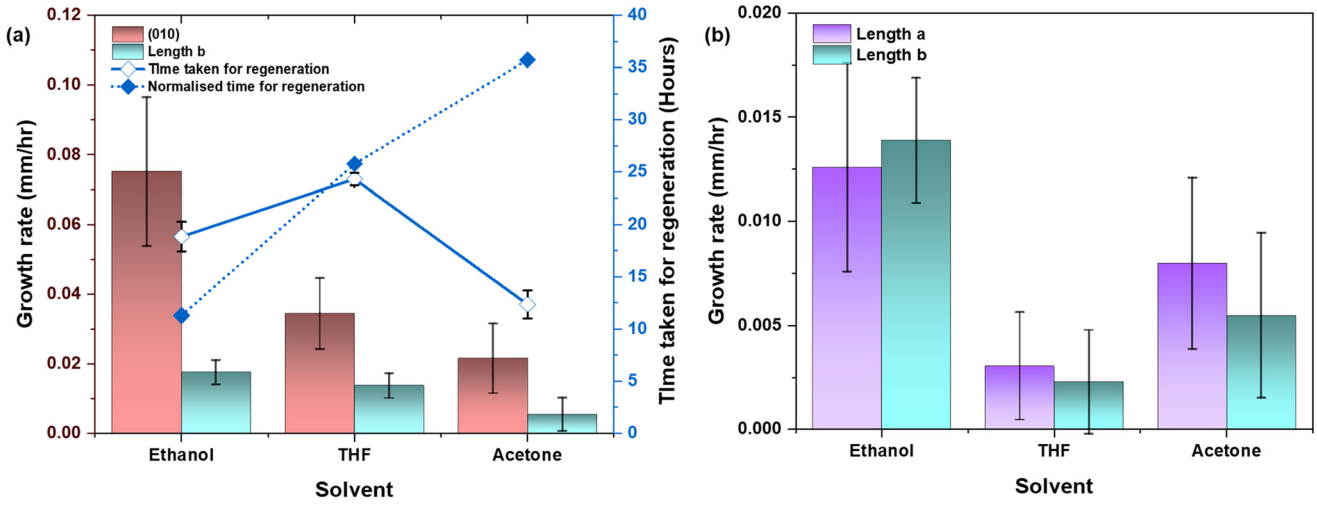

Fig. 10 (a) Growth rates of (010) and length *b* during regeneration along with the absolute and normalised time taken for regeneration in each solvent. (b) Growth rates of length *a* and *b* after regeneration in all three solvents. Error bars in each case represent the standard deviation.

Table 2 Fast and slow regeneration rates of paracetamol in different solvents at S = 1.10

Solvent	Rapid regeneration period h	% of total regeneration period	Rapid regeneration rate mm h^{-1}	Sluggish regeneration rate mm h^{-1}
Ethanol	1.60 ± 0.1	~9	0.16 ± 0.03	0.07 ± 0.02
THF	1.75 ± 0.2	~7	0.12 ± 0.02	0.04 ± 0.01
Acetone	2.00 ± 0.2	~16	0.07 ± 0.02	0.02 ± 0.01

rapidly (rapid regeneration). As regeneration progresses and new facets begin to form on the crystal, competition for solute molecules increases, resulting in a reduced overall regeneration rate (sluggish regeneration). However, even during the slow regeneration phase, the growth of (0 1 0) dominates over the growth of other facets. In this study, growth rates of (0 1 0) were further analysed to validate the two-step regeneration behaviour under various solvents and controlled conditions. As seen from Fig. 9, for each solvent there was indeed an initial part on the (0 1 0) growth curve that has a steeper slope compared to the rest of the regeneration phase. The duration and growth rates of which have been tabulated in Table 2. It is interesting to note that regardless of the total regeneration period, the fast regeneration phase only lasted for around 2 hours for each solvent, corresponding to around 8.5%, 7%, and 16% of the total regeneration period in ethanol, THF, and acetone respectively. However, the growth rates in this initial phase varied depending on the solvent, and followed the same trend as the overall regeneration rate: the fastest in ethanol (0.16 mm h^{-1}), followed by THF (0.12 mm h^{-1}), and lastly acetone (0.07 mm h^{-1}). These rates were at least twice as fast as the slower regeneration rates.

Discussion

The order of relative polarity across the solvents is as follows: ethanol > acetone > THF. It was therefore hypothesised that, since the (0 1 0) facet is an apolar facet,[20] the least polar solvent (THF) would have the highest affinity to the surface and hence result in a larger barrier to regeneration as more energy would be required to remove the solvent layer. However, this did not correlate with the case at hand. Based on the regeneration rates in the above sections, regeneration was the fastest in ethanol, followed by THF and then acetone. To elucidate this discrepancy, the interaction energy between the solvent and (0 1 0) crystal surface was calculated using molecular dynamic simulations and can be found in Table 3.

The interaction energy of THF was almost 7% lower than of acetone which was similarly lower than of ethanol. This suggested stronger bonding between (0 1 0) and THF followed by acetone and then weakest with ethanol. Molecules at the surface behave differently to those in the bulk because they are not fully surrounded by neighbouring atoms. Thus, the topmost layer of the crystal was unfixed during the simulations whilst keeping the lower layers fixed. This also leads to surface relaxation where the top layer of atoms slightly adjusts its positions to minimize surface energy, therefore more accurately capturing the real physical behaviour of the crystal. Snapshots of the bilayer after the MD simulation were taken to analyse the bonding between the solvent molecules and the paracetamol molecules on the surface (Fig. 11). Although (0 1 0) has no hydrogen bonding potential in the b direction, the unfixed solute layer has some degree of movement, thus, acetone and THF both formed hydrogen bonds with the surface molecules (Fig. 11(b) and (c)) but ethanol did not (Fig. 11(a)).

Although acetone and THF have higher dipole moments compared to ethanol, they are polar aprotic solvents, whereas ethanol is a polar protic solvent capable of independently forming hydrogen bonds. Since THF and acetone can only accept hydrogen bonds, it is postulated that the C–O–C group in THF and the C═O group in acetone preferentially bond with the hydroxyl (OH) groups of paracetamol molecules, reducing the probability of hydrogen bonding during crystallisation between free paracetamol molecules in solution and the (010) surface in the a and c direction. Conversely, in ethanol, it is energetically more favourable for the ethanol molecules to engage in hydrogen bonding with each other, interacting with paracetamol primarily through van der Waals and coulombic interactions. This can also be seen *via* the radial distribution function (RDF) for each system, as shown in Fig. 12. The lack of prominent peaks in the RDF curves, particularly in the case of ethanol, reflects the absence of strong, directional interactions—such as hydrogen bonding—between the ethanol molecules and the (010) crystal surface. In this case, coulombic interactions ($r \geq 5$ Å) dominate, which leads to more diffuse RDF features rather than distinct peaks. For THF and acetone, small peaks were observed, corresponding to potential hydrogen bonding ($r \leq 3$ Å) at r = 2.95 and 2.35 respectively, and van der Waals interactions ($3 \leq r \leq 5$ Å), albeit weaker in intensity compared to what might be seen with systems designed for strong surface binding.

The role of solvents in crystal growth is highly complex and influenced by multiple interdependent factors, not just the hydrogen bonding affinity to the surface, though this is

Table 3 Interaction energy between solvent and (0 1 0) crystal surface along with the solvent dielectric constant and molecular weight

Solvent	Interaction energy kcal mol^{-1}	Dipole moment	Molecular weight g mol^{-1}
Ethanol	−220.9	1.69	46.1
Acetone	−237.5	2.88	58.1
THF	−255.0	1.75	72.1

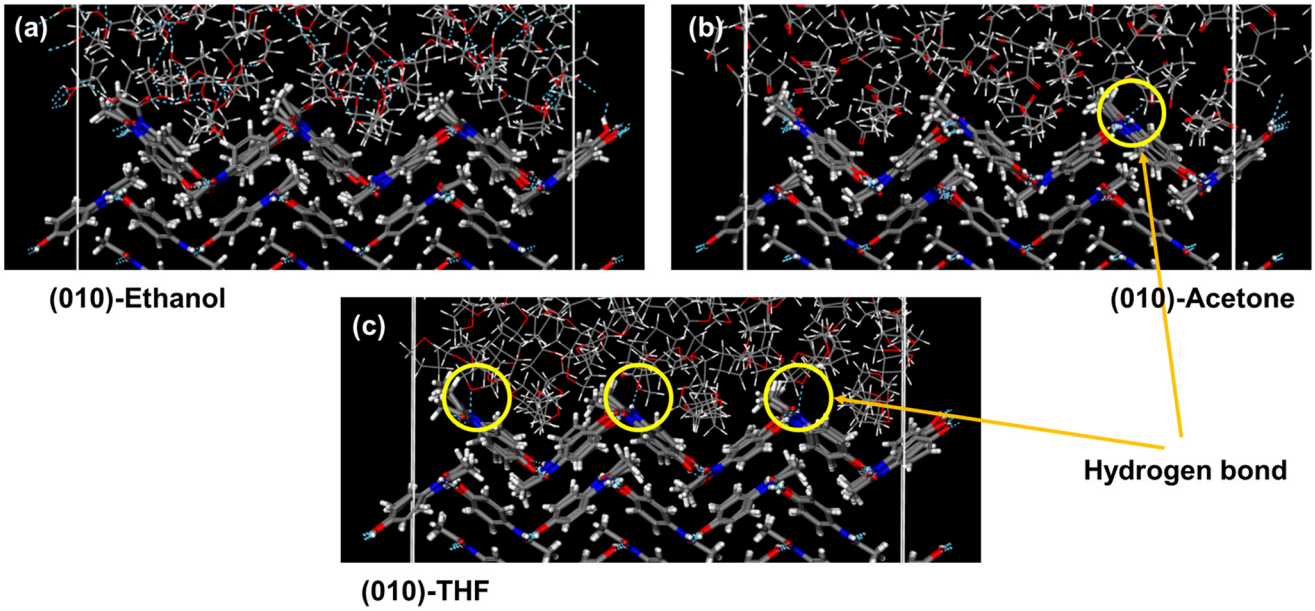

Fig. 11 Snapshots of the bilayer at the end of the MD simulations depicting the bonding between the top layer of (010) surface with (a) ethanol, (b) acetone, (c) THF.

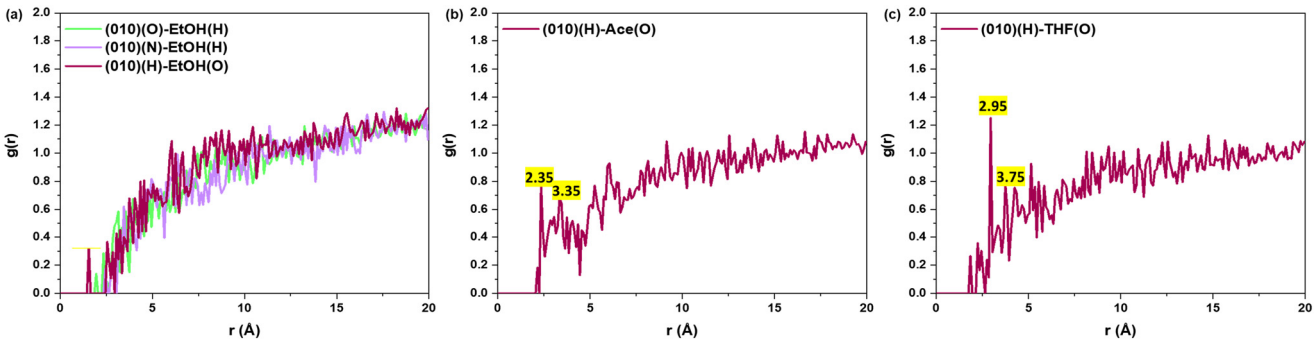

Fig. 12 RDF analysis of the bonding between the (010) surface and (a) ethanol, (b) acetone, and (c) THF.

often emphasised in the literature. Factors such as solubility, the rate of supersaturation generation, solvent pH, and evaporation number all contribute to the growth rate.[23] As shown in Table 1, the initial temperature across all solvent systems was consistent at 30 °C, as was the crystallisation temperature, T_c. With a constant supersaturation ratio of 1.10, the ratio of c to c^* remained the same in each case. Additionally, the gradient of the solubility curves between 25 °C and 30 °C was similar for all three solvents, resulting in only a marginal difference in Δc. Consequently, the amount of excess solute at 1.10 supersaturation available for growth in a 60 ml volume was also approximately 1 gram, regardless of the solvent.

The primary difference, however, stems from the solubility of paracetamol in these solvents. Keeping all other crystallisation variables constant, the inherent differences in solubility mean that the available solute for growth varies. For instance, the concentration of paracetamol in acetone was nearly 50% lower than in ethanol and 30% lower than in THF. Thus, while sufficient solute was present for crystal growth in each case, the ratio between solvent and solute molecules in solution differed, leading to a higher likelihood of favourable interactions in solvents with higher solubility.[55] This is particularly relevant during the regeneration phase when the (0 1 0) crystal face interacts with the solvent. After regeneration is complete and the (0 1 0) face disappears, the trend reverses, with growth rates in acetone surpassing those in THF, highlighting once again, the dominance of solute–solvent interactions with the morphologically important facets.

Conclusion

This study demonstrated the effect of solvents on crystal regeneration. Two key insights emerged: first, the pre-breakage crystal shape significantly influences regeneration time, highlighting the role of solute–solvent interactions in defining initial crystal habits. However, upon cleavage, the (0

1 0) facet dominates growth, with its rate governed primarily by the solubility of paracetamol in each solvent rather than specific solvent interactions. Higher solubility facilitates faster regeneration due to enhanced solute–crystal surface interactions. Interestingly, after the (0 1 0) facet disappears, solvent interactions regain control, once again dictating overall growth behaviour as seen in unbroken crystals. Overall, not only do the findings provide mechanistic insights into the role of solvents in crystal regeneration, but also the methodologies developed in this study offer a powerful framework for studying crystal growth dynamics in real time, enabling improved data acquisition for crystal growth post breakage.

Author contributions

Conceptualization, I. B., and J. Y. Y. H.; methodology, I. B. and D. E.; sample preparation, I. B., and D. E.; validation, I. B., and D. E.; formal analysis, I. B., and D. E.; investigation, I. B. and D. E.; resources, J. Y. Y. H.; data curation, I. B., and D. E.; writing – original draft preparation, I. B. and D. E.; writing – review and editing, I. B., D. E., and J. Y. Y. H.; visualization, I. B., D. E., and J. Y. Y. H.; supervision, J. Y. Y. H.; project administration, J. Y. Y. H.; funding acquisition, J. Y. Y. H. All authors have read and agreed to the published version of the manuscript.

Conflicts of interest

There are no conflicts to declare.

Data availability

Supplementary information: supplementary information (SI) containing the solubility data of paracetamol, details of the MATLAB image analysis as well as the molecular dynamic simulations, is available. See DOI: **https://doi.org/10.1039/D5CE00353A**.

The data, including regenerating crystal videos, supporting this article have been included as part of the supplementary information (SI). The MATLAB image analysis script used in this article is available upon request.

Acknowledgements

D. E. acknowledges the Department of Chemical Engineering at Imperial College London for a PhD Departmental Scholarship, as well as BASF (PA6590) for their funding. The authors gratefully acknowledge Ms. Allison Arber for her valuable assistance during the initial stages of this work. The authors also extend their thanks to Dr. Hamish Mitchel for his contribution in developing the Python protocol necessary for Dobot data acquisition. Additionally, the authors appreciate the insightful scientific discussions with Dr. Vivek Verma and Dr. Ethan Errington on molecular modelling.

References

1 R. Li, X. Zhang, H. Dong, Q. Li, Z. Shuai and W. Hu, Gibbs-Curie-Wulff Theorem in Organic Materials: A Case Study on the Relationship between Surface Energy and Crystal Growth, *Adv. Mater.*, 2016, **28**(8), 1697–1702.
2 R. Docherty, G. Clydesdale, K. J. Roberts and P. Bennema, Application of bravais-friedel-donnay-harker, attachment energy and ising models to predicting and understanding the morphology of molecular crystals, *J. Phys. D: Appl. Phys.*, 1991, **24**(2), 89–99.
3 J. Willard Gibbs, *Scientific Papers of J. Willard Gibbs*, Longmans, Green, and Co., 1906.
4 M. A. Lovette, A. R. Browning, D. W. Griffin, J. P. Sizemore, R. C. Snyder and M. F. Doherty, Crystal shape engineering, *Ind. Eng. Chem. Res.*, 2008, **47**(24), 9812–9833.
5 A. Chernov, The kinetics of the growth forms of crystals, *Sov. Phys. Crystallogr.*, 1963, **7**, 728–730.
6 F. C. Frank, On the kinematic theory of crystal growth and dissolution processes, ii, *Z. Phys. Chem.*, 1972, **77**(1–6), 84–92.
7 D. S. Coombes, C. R. A. Catlow, J. D. Gale, M. J. Hardy and M. R. Saunders, Theoretical and experimental investigations on the morphology of pharmaceutical crystals, *J. Pharm. Sci.*, 2002, **91**(7), 1652–1658.
8 J. D. H. Donnay and D. Harker, A New Law of Crystal Morphology Extending the Law of Bravais, *Am. Mineral.*, 1937, **22**, 446.
9 A. Bravais, *Études cristallographiques, Gauthier-Villars*, Paris, France, 1913.
10 G. Friedel, *Leçons de cristallographie*, A. Hermann, Paris, France, 1911.
11 P. Hartman and W. G. Perdok, On the relations between structure and morphology of crystals. I, *Acta Crystallogr.*, 1955, **8**(1), 49–52.
12 P. Hartman and P. Bennema, The attachment energy as a habit controlling factor. I. Theoretical considerations, *J. Cryst. Growth*, 1980, **49**(1), 145–156.
13 G. Chen, C. Chen, M. Xia, W. Lei, F. Wang and X. Gong, A study of the solvent effect on the crystal morphology of hexogen by means of molecular dynamics simulations, *RSC Adv.*, 2015, **5**(32), 25581–25589.
14 D. Zhu, S. Zhang, P. Cui, C. Wang, J. Dai and L. Zhou, *et al.*, Solvent effects on catechol crystal habits and aspect ratios: A combination of experiments and molecular dynamics simulation study, *Crystals*, 2020, **10**(4), 316.
15 M. Salvalaglio, T. Vetter, F. Giberti, M. Mazzotti and M. Parrinello, Uncovering Molecular Details of Urea Crystal Growth in the Presenceof Additives, *J. Am. Chem. Soc.*, 2012, **134**, 17221–17233.
16 S. Piana, M. Reyhani and J. D. Gale, Simulating micrometre-scale crystal growth from solution, *Nature*, 2005, **438**(7064), 70–73.
17 M. Salvalaglio, T. Vetter, M. Mazzotti and M. Parrinello, Controlling and predicting crystal shapes: The case of urea, *Angew. Chem., Int. Ed.*, 2013, **52**(50), 13369–13372.

18 E. M. Peters, M. Svärd and K. Forsberg, Impact of process parameters on product size and morphology in hydrometallurgical antisolvent crystallization, *CrystEngComm*, 2022, **24**(15), 2851–2866.
19 A. Lynch, V. Verma, J. Zeglinski, P. Bannigan and Å. Rasmuson, Face indexing and shape analysis of salicylamide crystals grown in different solvents, *CrystEngComm*, 2019, **21**(16), 2648–2659.
20 J. Y. Y. Heng, A. Bismarck, A. F. Lee, K. Wilson and D. R. Williams, Anisotropic Surface Energetics and Wettability of Macroscopic Form I Paracetamol Crystals, *Langmuir*, 2006, **22**, 2760–2769.
21 J. Y. Y. Heng and D. R. Williams, Wettability of paracetamol polymorphic forms i and II, *Langmuir*, 2006, **22**(16), 6905–6909.
22 R. Ho, S. J. Hinder, J. F. Watts, S. E. Dilworth, D. R. Williams and J. Y. Y. Heng, Determination of surface heterogeneity of d-mannitol by sessile drop contact angle and finite concentration inverse gas chromatography, *Int. J. Pharm.*, 2010, **387**(1–2), 79–86.
23 C. Sudha and K. Srinivasan, Understanding the effect of solvent polarity on the habit modification of monoclinic paracetamol in terms of molecular recognition at the solvent crystal/interface, *Cryst. Res. Technol.*, 2014, **49**(11), 865–872.
24 N. Shahrir, N. Anuar, N. A. Abdul Muttalib, S. N. A. Yusop, M. R. Abu Bakar and F. Adam, *et al.*, The Role of Solvent Hydroxyl Functional Groups on the Interaction Energy and Growth of Form i Paracetamol Crystal Facets, *Org. Process Res. Dev.*, 2022, **26**(12), 3226–3235.
25 J. Li and M. F. Doherty, Steady state morphologies of paracetamol crystal from different solvents, *Cryst. Growth Des.*, 2017, **17**(2), 659–670.
26 R. I. Ristic, S. Finnie, D. B. Sheen and J. N. Sherwood, Macro- and micromorphology of monoclinic paracetamol grown from pure aqueous solution, *J. Phys. Chem. B*, 2001, **105**(38), 9057–9066.
27 V. Marinova, G. P. F. Wood, I. Marziano and M. Salvalaglio, Investigating the Role of Solvent in the Formation of Vacancies on Ibuprofen Crystal Facets, *Cryst. Growth Des.*, 2022, **22**(5), 3034–3041.
28 C. Stoica, P. Verwer, H. Meekes, P. J. C. M. Van Hoof, F. M. Kaspersen and E. Vlieg, Understanding the effect of a solvent on the crystal habit, *Cryst. Growth Des.*, 2004, **4**(4), 765–768.
29 D. Winn and M. F. Doherty, Modeling crystal shapes of organic materials grown from solution, *AIChE J.*, 2000, **46**(7), 1348–1367.
30 K. V. R. Prasad, R. I. Ristic, D. B. Sheen and J. N. Sherwood, Dissolution kinetics of paracetamol single crystals, *Int. J. Pharm.*, 2002, **238**, 29–41.
31 B. Szilágyi and B. G. Lakatos, Model-based analysis of stirred cooling crystallizer of high aspect ratio crystals with linear and nonlinear breakage, *Comput. Chem. Eng.*, 2017, **98**, 180–196.
32 Y. Zhang and M. F. Doherty, Simultaneous prediction of crystal shape and size for solution crystallization, *AIChE J.*, 2004, **50**(9), 2101–2112.
33 Z. K. Nagy, G. Fevotte, H. Kramer and L. L. Simon, Recent advances in the monitoring, modelling and control of crystallization systems, *Chem. Eng. Res. Des.*, 2013, **91**(10), 1903–1922.
34 L. Bosetti and M. Mazzotti, Population Balance Modeling of Growth and Secondary Nucleation by Attrition and Ripening, *Cryst. Growth Des.*, 2020, **20**(1), 307–319.
35 R. Tyrrell and P. Frawley, Single crystal fragmentation: Visualizing breakage model performance for pharmaceutical processes, *Wear*, 2018, **414–415**, 275–288.
36 S. B. Gadewar and M. F. Doherty, A dynamic model for evolution of crystal shape, *J. Cryst. Growth*, 2004, **267**(1–2), 239–250.
37 S. A. Schiele, T. Haider and H. Briesen, Growth of broken crystals tracked in 4D using X-ray computed tomography and its influence on impurity incorporation, *Sci. Rep.*, 2024, **14**(1), 1–14.
38 C. Y. Ma and K. J. Roberts, Morphological population balance modelling of the effect of crystallisation environment on the evolution of crystal size and shape of para-aminobenzoic acid, *Comput. Chem. Eng.*, 2019, **126**, 356–370.
39 H. Li and B. S. Yang, Model evaluation of particle breakage facilitated process intensification for Mixed-Suspension-Mixed-Product-Removal (MSMPR) crystallization, *Chem. Eng. Sci.*, 2019, **207**, 1175–1186.
40 I. Bade, V. Verma, I. Rosbottom and J. Y. Y. Heng, Crystal regeneration - a unique growth phenomenon observed in organic crystals post breakage, *Mater. Horiz.*, 2023, 1425–1430.
41 A. Nong, C. Schleper, A. Martin, M. Paolello, F. L. Nordstrom and G. Capellades, Impurity Retention and Pharmaceutical Solid Solutions: Visualizing the Effect of Impurities on Dissolution and Growth using Dyed Crystals, *CrystEngComm*, 2024, **26**(38), 5337–5350.
42 L. Jiang, W. Chen, L. Zhou, L. Xu, F. He and J. Y. Y. Heng, *et al.*, Uncovering crystal growth and regeneration mechanism to control crystal morphology: The case study of aceclofenac, *Sep. Purif. Technol.*, 2024, **347**, 127577.
43 W. Omar, S. Al-Sayed, A. Sultan and J. Ulrich, Growth rate of single acetaminophen crystals in supersaturated aqueous solution under different operating conditions, *Cryst. Res. Technol.*, 2008, **43**(1), 22–27.
44 T. T. H. Nguyen, R. B. Hammond, K. J. Roberts, I. Marziano and G. Nichols, Precision measurement of the growth rate and mechanism of ibuprofen {001} and {011} as a function of crystallization environment, *CrystEngComm*, 2014, **16**(21), 4568–4586.
45 C. A. Offiler, A. J. Cruz-Cabeza, R. J. Davey and T. Vetter, Crystal Growth Cell Incorporating Automated Image Analysis Enabling Measurement of Facet Specific Crystal Growth Rates, *Cryst. Growth Des.*, 2022, **22**(5), 2837–2848.
46 C. Jiang, C. Y. Ma, T. A. Hazlehurst, T. P. Ilett, A. S. M. Jackson and D. C. Hogg, *et al.*, Automated Growth Rate Measurement of the Facet Surfaces of Single Crystals of the β-Form of l-Glutamic Acid Using Machine Learning Image Processing, *Cryst. Growth Des.*, 2024, **24**(8), 3277–3288.

47 L. Aisling and R. Åke, Crystal Growth of Single Salicylamide Crystals, *Cryst. Growth Des.*, 2019, **19**(12), 7230–7239.
48 R. Soto, V. Verma, A. Lynch, B. K. Hodnett and Å. C. Rasmuson, Crystal Growth Kinetics of Pharmaceutical Compounds, *Cryst. Growth Des.*, 2020, **20**(12), 7626–7639.
49 M. Haisa, S. Kashino, R. Kawai and H. Maeda, The Monoclinic Form of p-Hydroxyacetanilide, *Acta Crystallogr., Sect. B*, 1976, **30**, 1283–1285.
50 R. A. Granberg and Å. C. Rasmuson, Solubility of paracetamol in pure solvents, *J. Chem. Eng. Data*, 1999, **44**(6), 1391–1395.
51 H. Sun, Compass: An ab initio force-field optimized for condensed-phase applications - Overview with details on alkane and benzene compounds, *J. Phys. Chem. B*, 1998, **102**(38), 7338–7364.
52 S. L. Mayo, B. D. Olafson and W. A. Goddard, DREIDING: A generic force field for molecular simulations, *J. Phys. Chem.*, 1990, **94**(26), 8897–8909.
53 A. K. Rappé, C. J. Casewit, K. S. Colwell, W. A. Goddard and W. M. Skiff, UFF, a Full Periodic Table Force Field for Molecular Mechanics and Molecular Dynamics Simulations, *J. Am. Chem. Soc.*, 1992, **114**(25), 10024–10035.
54 H. C. Andersen, Molecular Dynamics Simulations at Constant Pressure and/or Temperature, *J. Chem. Phys.*, 1980, **72**(4), 2384–2393.
55 C. T. Óciardhá, N. A. Mitchell, K. W. Hutton and P. J. Frawley, Determination of the crystal growth rate of paracetamol as a function of solvent composition, *Ind. Eng. Chem. Res.*, 2012, **51**(12), 4731–4740.

